Supplementary Material for "Pressure Induced Topological Superconductivity in the Spin-Orbit Mott Insulator $GaTa_4Se_8$"

Moon Jip Park, GiBaik Sim, Min Yong Jeong, Archana Mishra, Myung Joon Han, and SungBin Lee
Department of Physics, KAIST, Daejeon 34141, Republic of Korea
(Dated: June 3, 2020)

1. *AB INITIO* PARAMETERS AND DFT CALCULATION DETAILS

The electronic structure calculations by using OPENMX were carried out with 400 Ry energy cutoff. In order to take into account of pressure effect, we used the experimental lattice parameters measured at 0 (ambient), 5, 10, and 14.5 GPa [1]. The tight-binding hopping parameters and the interaction parameters were estimated in between t_2 molecular orbitals. As shown in Fig. S1(a), MLWF-based tight-binding bands well reproduce the DFT-LDA results. Fig. S2(a) visualizes the calculated MLWFs denoted by D_{xy}, D_{yz}, and D_{zx} each of which is composed of four atomic d_{xy}, d_{yz}, and d_{zx} orbitals, respectively. Four major hopping parameters are presented in Table. I where we present the values obtained from ECALJ code [2]. This set of hopping parameters were double checked with OPENMX, and the deviations are found to be less than 1 meV.

Lattice structure	Pressure (GPa)	t_1(meV)	t_2(meV)	t_3(meV)	t'(meV)
Experimental	0	−55	28	7	14
	5	−65	31	7	14
	10	−73	35	5	15
	14.5	−78	36	4	15
Optimized (within DFT)[3]	0	−55.7	27.6	7.1	14.5

TABLE I. The calculated hopping parameters as a function of pressure. For the convention of each parameter, see Fig. S2 (c). It is found that the lattice optimization does not make significant changes.

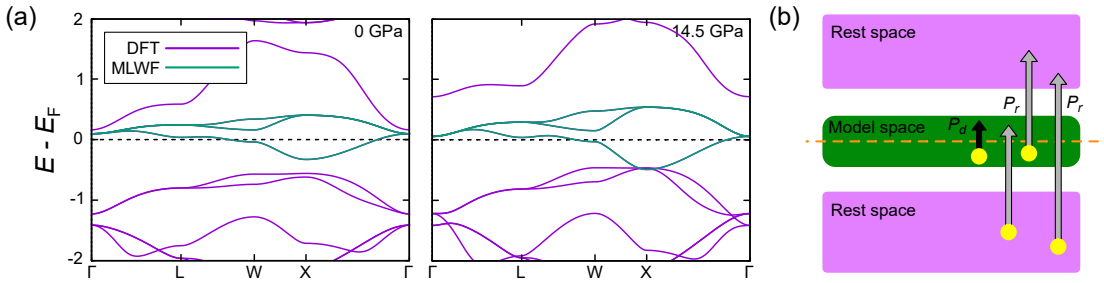

FIG. S1. (a) The calculated band dispersion by DFT-LDA (violet) and MLWF tight-binding parameters (green) at the pressure value of 0 (left) and 14.5 GPa (right). (b) Schematic diagram to describe the polarization in cRPA procedure. The black arrow represents the polarization within the (correlated) model space (P_d) while the gray ones refer to the other polarizations (P_r). In the current study, the correlated space is defined as molecular t_2 orbitals corresponding to the green-colored bands in (a).

In order to consider electron interactions, we performed cRPA calculations which can properly take into account of screening effects in solids [4–11] and give rise to the reliable estimation of effective 'on-site' interaction strengths being much smaller than the 'bare' interactions, $\mathcal{V}$. Within RPA, the fully screened interaction $\mathcal{U}$ can be calculated from

$$\mathcal{U} = \epsilon^{-1}\mathcal{V} \tag{S1}$$

where $\epsilon = 1 - \mathcal{V}P$ and P is the polarization [4]. In order to cooperate with correlated electron models (e.g., Hubbard model), the correlated orbitals or subspaces need to be defined properly. The effective Coulomb interaction U in such

Pressure (GPa)	U (eV)	U' (eV)	$J_{\rm H}$ (eV)	$\mathcal{U}$ (eV)	$\mathcal{U}'$ (eV)	$\mathcal{J}_{\rm H}$ (eV)
0 (ambient)	0.668	0.507	0.061	0.175	0.063	0.046
5	0.637	0.481	0.059	0.184	0.071	0.046
10	0.599	0.448	0.057	0.190	0.077	0.046
14.5	0.585	0.436	0.056	0.193	0.080	0.046

TABLE II. The calculated interaction parameters as a function of pressure. U, U', and $J_{\rm H}$ refers to the intra-, inter-orbital interaction, and the Hund coupling calculated by cRPA, respectively. The corresponding fully screened values are denoted by $\mathcal{U}$, $\mathcal{U}'$, and $\mathcal{J}_{\rm H}$, respectively.

a model can be represented by [4]

$$U = [1 - \mathcal{V}(P - P_d)]^{-1}\mathcal{V} = [1 - \mathcal{V}(P_r)]^{-1}\mathcal{V} \tag{S2}$$

where P_d and P_r refers to the polarization within the correlated orbitals and the other ('rest') space, respectively; see Fig. S1. The relationship between the fully screened interaction, $\mathcal{U}$, and the partially-screened ('constrained') U can be found by [4]

$$\mathcal{U} = [1 - \mathcal{V}(P_r + P_d)]^{-1}\mathcal{V} = [(1 - \mathcal{V}P_r)\{1 - (1 - \mathcal{V}P_r)^{-1}\mathcal{V}P_d\}]^{-1}\mathcal{V} \tag{S3}$$

$$= \{1 - (1 - \mathcal{V}P_r)^{-1}\mathcal{V}P_d\}^{-1}(1 - \mathcal{V}P_r)^{-}1\mathcal{V} = [1 - UP_d]^{-1}U. \tag{S4}$$

Our calculation results of these values are presented in Table. II.

It is noted that the strengths of 'on-site' Coulomb and Hund's interaction are smaller than the typical values for $5d$ transition metal ions. It is is reasonably well understood from the nature of molecular orbitals which are distributed over the four atomic Ta sites. According to a recent study, these interaction parameters get reduced by a factor of $\sim$1/4 [12]. The effect beyond this simple estimation such as the screenings of other molecular orbitals have been taken into account by our cRPA calculation.

2. TIGHT-BINDING MODEL DESCRIPTION

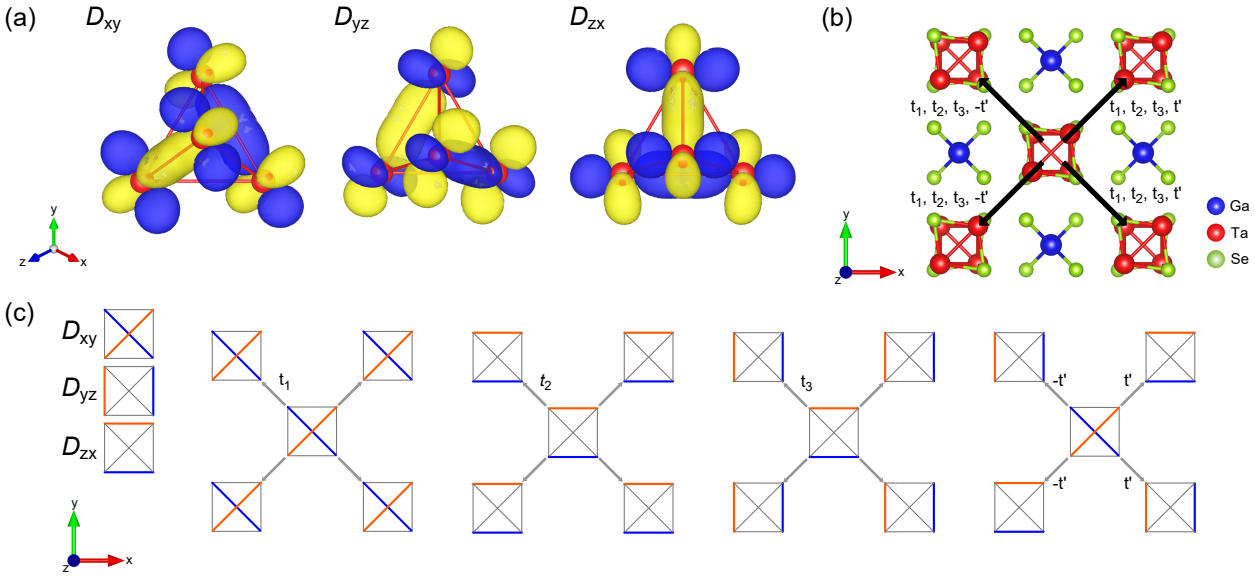

FIG. S2. (a) The calculated MLWFs of three molecular t_2 orbitals where we used the isosurface value of 0.05. (b) Top view of crystal structure which clearly shows the arrangement of Ta_4Se_4 and $GaSe_4$ clusters in the xy-plane. The hoppings in between Ta_4Se_4 cluster sites are depicted by black arrows which are orbital dependent. (c) The schematic figure to represent the orbital-dependent hoppings. The calculated four major hoppings, t_1, t_2, t_3, and t' are presented in Table. I.

In this section, we construct the tight binding model description for the completeness. We mainly repeat the description of Ref. 3 here. The starting point of our tight-binding model is the molecular t_2 orbitals (D_{xy}, D_{yz}, D_{zx}) basis. In the absence of the SOC, the nearest-neighbor hopping matrix from i site to j site can be generally written as,

$$\hat{T}_{\text{hopping};ij} = \begin{pmatrix} S_{11} & S_{12} - A_{12} & S_{13} + A_{13} \\ S_{12} + A_{12} & S_{22} & S_{23} - A_{23} \\ S_{13} - A_{13} & S_{23} + A_{23} & S_{33} \end{pmatrix} \tag{S5}$$

Here, we separate the inversion even and odd hopping components as S and A respectively. According to the Wannier function analysis, there exist four distinct hopping channels t_1, t_2, t_3, and t'. The inversion even hopping terms, t_1, t_2, and t_3, correspond to t_{dd1} (σ-type), t_{pd} (π-type), and t_{dd2} (δ-type) hopping integrals (See Figure S2). In addition, the inversion odd term t' is allowed due to the lack of inversion symmetry. In terms of the hopping matrix defined in Eq. (S5), the matrix elements are explicitly given as,

$$\begin{aligned}
(n_1, n_2, n_3) = (\pm 1, 0, 0) \quad & S_{11} = t_1,\ S_{22} = S_{33} = t_2,\ S_{23} = -t_3,\ A_{13} = -A_{12} = \mp t' \\
(n_1, n_2, n_3) = (0, \pm 1, 0) \quad & S_{11} = S_{33} = t_2,\ S_{22} = t_1,\ S_{13} = -t_3,\ A_{12} = -A_{23} = \mp t' \\
(n_1, n_2, n_3) = (0, 0, \pm 1) \quad & S_{11} = S_{22} = t_2,\ S_{33} = t_1,\ S_{12} = -t_3,\ A_{13} = -A_{23} = \pm t' \\
(n_1, n_2, n_3) = (\pm 1, \mp 1, 0) \quad & S_{11} = S_{22} = t_2,\ S_{33} = t_1,\ S_{12} = t_3,\ A_{13} = A_{23} = \pm t' \\
(n_1, n_2, n_3) = (0, \pm 1, \mp 1) \quad & S_{11} = t_1,\ S_{22} = S_{33} = t_2,\ S_{23} = t_3,\ A_{13} = A_{12} = \pm t' \\
(n_1, n_2, n_3) = (\pm 1, 0, \mp 1) \quad & S_{11} = S_{33} = t_2,\ S_{22} = t_1,\ S_{13} = t_3,\ A_{12} = A_{23} = \mp t'
\end{aligned} \tag{S6}$$

where (n_1, n_2, n_3) characterizes the direction of the hopping, $\mathbf{r}_{ij} = n_1\mathbf{a}_1 + n_2\mathbf{a}_2 + n_1\mathbf{a}_2$. $\mathbf{a_{1,2,3}}$ are the unit vectors of the FCC lattice. We now include the SOC effect in the Hamiltonian as,

$$\hat{H}_{\text{SOC}} = \lambda_{\text{SO}} \mathbf{L} \cdot \mathbf{S}. \tag{S7}$$

where λ_{SO} is the strength of the SOC. and $\mathbf{L}$ and $\mathbf{S}$ are the orbital and the spin angular momentum operators, respectively. We can rewrite the Hamiltonian in Eq. (S5) in terms of j_{eff} basis:

$$\begin{aligned}
|j_{\text{eff}} = \frac{1}{2}, m = \frac{1}{2}\rangle &= \frac{1}{\sqrt{3}}|D_{yz}\downarrow\rangle + \frac{i}{\sqrt{3}}|D_{xz}\downarrow\rangle + \frac{1}{\sqrt{3}}|D_{xy}\uparrow\rangle, \\
|j_{\text{eff}} = \frac{1}{2}, m = -\frac{1}{2}\rangle &= \frac{1}{\sqrt{3}}|D_{yz}\downarrow\rangle - \frac{i}{\sqrt{3}}|D_{xz}\downarrow\rangle - \frac{1}{\sqrt{3}}|D_{xy}\uparrow\rangle, \\
|j_{\text{eff}} = \frac{3}{2}, m = \frac{3}{2}\rangle &= -\frac{1}{\sqrt{2}}|D_{yz}\uparrow\rangle - \frac{i}{\sqrt{2}}|D_{xz}\uparrow\rangle, \\
|j_{\text{eff}} = \frac{3}{2}, m = \frac{1}{2}\rangle &= -\frac{1}{\sqrt{6}}|D_{yz}\downarrow\rangle - \frac{i}{\sqrt{6}}|D_{xz}\downarrow\rangle + \sqrt{\frac{2}{3}}|D_{xy}\uparrow\rangle, \\
|j_{\text{eff}} = \frac{3}{2}, m = -\frac{1}{2}\rangle &= \frac{1}{\sqrt{6}}|D_{yz}\uparrow\rangle - \frac{i}{\sqrt{6}}|D_{xz}\uparrow\rangle + \sqrt{\frac{2}{3}}|D_{xy}\downarrow\rangle, \\
|j_{\text{eff}} = \frac{3}{2}, m = -\frac{3}{2}\rangle &= \frac{1}{\sqrt{2}}|D_{yz}\downarrow\rangle - \frac{i}{\sqrt{2}}|D_{xz}\downarrow\rangle,
\end{aligned}$$

where the arrows indicate the electron spin. In j_{eff} basis, the hopping matrix and the on-site SOC term transforms as,

$$\hat{T}_{\text{hopping};ij} = \begin{pmatrix} T_{ij}^{1/2} & \Theta_{ij} \\ \Theta_{ij}(-A)^\dagger & T_{ij}^{3/2} \end{pmatrix}, \ \hat{H}_{\text{SOC}} = \begin{pmatrix} +\lambda_{\text{SO}} I_2 & 0 \\ 0 & -\frac{1}{2}\lambda_{\text{SO}} I_4 \end{pmatrix}. \tag{S8}$$

where I_n are n-dimensional identity matrix. $T^{1/2(3/2)}$ describes the intraband hopping terms of $j_{\text{eff}} = 1/2$ (3/2) bands, and Θ represents the interband tunnelings. The explicit forms of the hopping matrices follow Eq. (S5). If the energy splitting between the $j_{\text{eff}} = 1/2$ and 3/2 bands, $\frac{3}{2}\lambda_{\text{SO}}$, is large compared to the inter-orbital hopping terms Θ, $j_{\text{eff}} = 1/2$ and 3/2 subsectors effectively decouples.

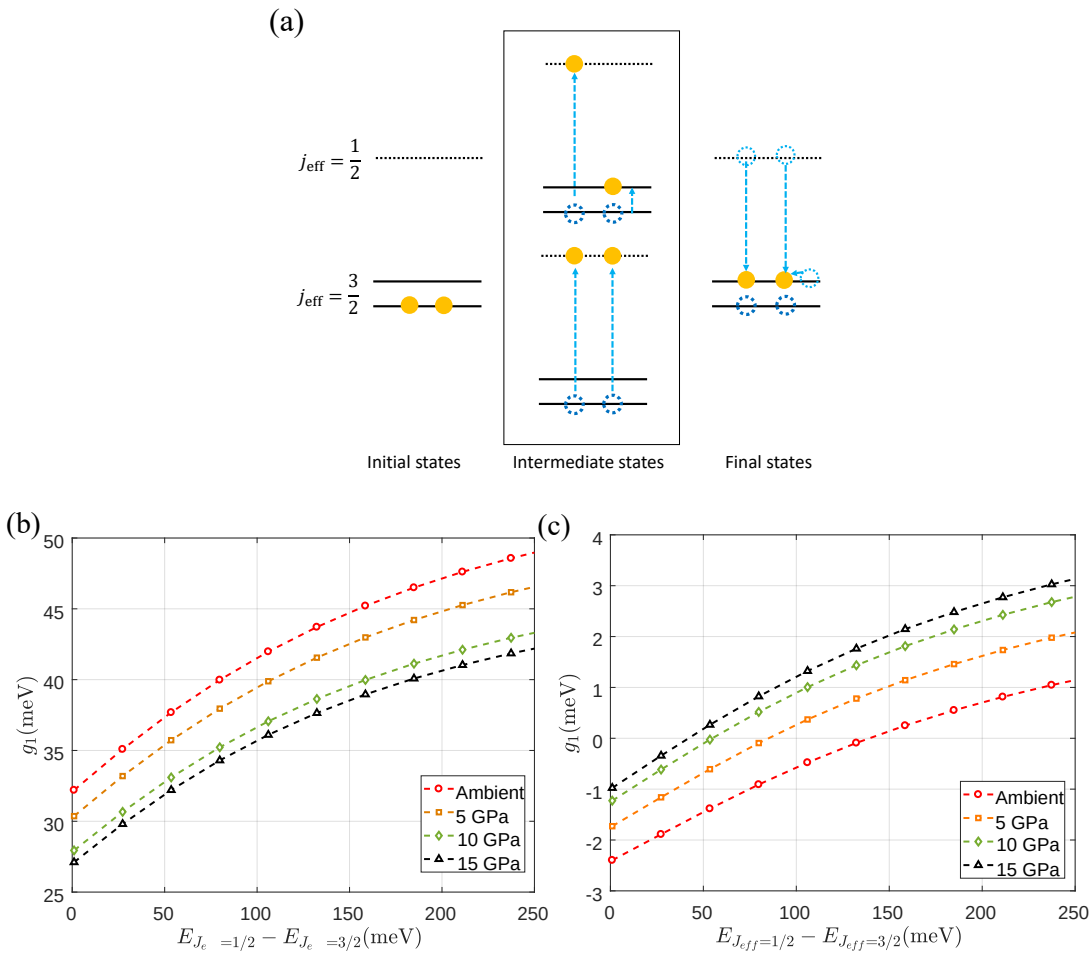

FIG. S3. (a) Schematic representation of the interband tunneling process. The second-order process mediating the intermediate $j_{\text{eff}} = 1/2$ states contributes to the effective $j_{\text{eff}} = 3/2$ many-body interactions (b-c) $j_{\text{eff}} = 3/2$ projected pairing interaction strength derived from the exact diagonalization result using (b) the cRPA and (c) the fully screened values of the interaction parameters. We find that the reduction of the band splitting decreases the pairing constants, g_1.

3. PROJECTION TO $j_{\text{eff}} = 3/2$ BASIS

In this section, we project the interacting Hamiltonian to $j_{\text{eff}} = 3/2$ basis. We start our analysis by writing down the interacting Hamiltonian as,

$$\begin{aligned} H_I &= U \sum_{iu} n_{iu\uparrow} n_{iu\downarrow} + U' \sum_{iu,v<u} n_{iu\sigma} n_{iv\sigma'} + \frac{J_H}{2} \sum_{iu\neq v,\sigma,\sigma'} d^\dagger_{iu\sigma} d^\dagger_{iv\sigma'} d_{iu\sigma'} d_{iv\sigma} + \frac{J_H}{2} \sum_{iu\neq v,\sigma\neq\sigma'} (d^\dagger_{iu\sigma} d^\dagger_{iu\sigma'} d_{iv\sigma'} d_{iv\sigma} + h.c.) \\ &= H_U + H_{U'} + H_{J1} + H_{J2} \end{aligned} \tag{S9}$$

where i is the site index, $u, v \in (xy, yz, zx)$ denote the orbital indices (D_{xy}, D_{yz}, D_{zx}) and $\sigma, \sigma' \in (\uparrow, \downarrow)$ are spin indices. Here, $n_{iu\sigma} = d^\dagger_{iu\sigma} d_{iu\sigma}$ is the number operator and $d_{iu\sigma}$ $(d^\dagger_{iu\sigma})$ are the annihilation (creation) operator of electrons at site i and orbital u with spin σ. U and U' represent the intra-orbital and inter-orbital interaction strengths respectively. The third and fourth terms are the Hund exchange interaction and Hund pair hopping interaction respectively parametrized by J. With $(U, U', J) > 0$, these interaction terms are repulsive in nature.

A. $j_{\text{eff}} = 3/2$ intra-band contribution

Due to spin orbit coupling, in the absence of interactions, the degenerate t_2 orbital states split into $J = 1/2$ doublet with energy λ and $J = 3/2$ quartet with energy $-\lambda/2$. Large λ leads to the large energy gap between these states with negligible mixing. Hence, we restrict to $J = 3/2$ manifold and project the interacting Hamiltonian H_I, given in Eq. (S9), to the $J = 3/2$ basis states. Any operator O expressed in terms of spins and orbitals are projected to the $J = 3/2$ subspace through the projection operator $P_{3/2}$ and the projected operator is denoted as $\tilde{O} \equiv P_{3/2}OP_{3/2}$. Thus, the projection of the number operators $n_{\alpha\beta}$, spin operators $\mathbf{S}_{\alpha\beta} = (S^x_{\alpha\beta}, S^y_{\alpha\beta}, S^z_{\alpha\beta})$ to the $J = 3/2$ subspace can be written as

$$\begin{aligned}
\tilde{n}_{\alpha\beta} &= P_{3/2} n_{\alpha\beta} P_{3/2} = \Psi^\dagger \Big(\frac{3}{4} I - \frac{J_\gamma^2}{3}\Big)\Psi \\
\tilde{S}^\gamma_{\alpha\beta} &= P_{3/2} S^\gamma_{\alpha\beta} P_{3/2} = \Psi^\dagger \Big(\frac{3}{4} J_\gamma - \frac{J_\gamma^3}{3}\Big)\Psi \\
\tilde{S}^{\alpha(\beta)}_{\alpha\beta} &= P_{3/2} S^{\alpha(\beta)}_{\alpha\beta} P_{3/2} = \Psi^\dagger \Big(\frac{1}{4} J_{\alpha(\beta)} - \frac{J_\gamma J_{\alpha(\beta)} J_\gamma}{3}\Big)\Psi
\end{aligned} \tag{S10}$$

where $\alpha, \beta, \gamma \in (x, y, z)$ with $\alpha \neq \beta \neq \gamma$ and the orbital index u in Eq. (S9) can be represented as $u = \alpha\beta$. $\mathbf{J} = (J_x,\ J_y,\ J_z)$ and I is the 4×4 identity matrix. $\Psi = [d_{3/2}\ d_{1/2}\ d_{-1/2}\ d_{-3/2}]^T$ is the four component spinor where d_{m_j} is the annihilation operator of electrons in angular momentum state $|J = 3/2, m_j\rangle$ and $m_j = (3/2,\ 1/2, -1/2, -3/2)$ with J_z being diagonal in this basis. The projected interacting Hamiltonian is written as,

$$\tilde{H}_I = \tilde{H}_U + \tilde{H}_{U'} + \tilde{H}_{J1} + \tilde{H}_{J2} \tag{S11}$$

which is a 4×4 matrix. Hence, we can express the projected interacting Hamiltonian in terms of the Dirac gamma matrices. In our work, the gamma matrices are explicitly given as following:

$$\gamma_1 = \sigma^z \otimes \sigma^y,\ \gamma_2 = \sigma^z \otimes \sigma^x,\ \gamma_3 = \sigma^y \otimes I_{2\times2},\quad \gamma_4 = \sigma^x \otimes I_{2\times2},\quad \gamma_5 = \sigma^z \otimes \sigma^z \tag{S12}$$

where $\sigma = (\sigma^x,\ \sigma^y,\ \sigma^z)$ are the Pauli matrices. Using the gamma matrices, we can define the time-reversal operator as, $T = \gamma_1\gamma_3 K$ where K is the complex conjugate operator. The projected interacting Hamiltonian can, thus, be written as

$$\begin{aligned}
\tilde{H}_U &= \frac{U}{24}\Big[2(\Psi^\dagger\Psi)^2 + (\Psi^\dagger\gamma_4\Psi)^2 + (\Psi^\dagger\gamma_5\Psi)^2 - 2(\Psi^\dagger\gamma_{12}\Psi)^2 - (\Psi^\dagger\gamma_{34}\Psi)^2 - (\Psi^\dagger\gamma_{35}\Psi)^2\Big] \\
\tilde{H}_{U'} &= \frac{U'}{12}\Big[4(\Psi^\dagger\Psi)^2 - (\Psi^\dagger\gamma_4\Psi)^2 - (\Psi^\dagger\gamma_5\Psi)^2\Big] \\
\tilde{H}_{J1} &= \frac{-J}{72}\Big[12(\Psi^\dagger\Psi)^2 - 3(\Psi^\dagger\gamma_4\Psi)^2 - 3(\Psi^\dagger\gamma_5\Psi)^2 - 4(\Psi^\dagger\gamma_{12}\Psi)^2 - 4(\Psi^\dagger\gamma_{13}\Psi)^2 - (\Psi^\dagger\gamma_{14}\Psi)^2 + 3(\Psi^\dagger\gamma_{15}\Psi)^2 - 4(\Psi^\dagger\gamma_{23}\Psi)^2 \\
&\quad - (\Psi^\dagger\gamma_{24}\Psi)^2 + 3(\Psi^\dagger\gamma_{25}\Psi)^2 + 5(\Psi^\dagger\gamma_{34}\Psi)^2 - 3(\Psi^\dagger\gamma_{35}\Psi)^2\Big] - \frac{J}{18}\Big[2(\Psi^\dagger\gamma_{12}\Psi)(\Psi^\dagger\gamma_{34}\Psi) - (\Psi^\dagger\gamma_{23}\Psi)(\Psi^\dagger\gamma_{14}\Psi) \\
&\quad + (\Psi^\dagger\gamma_{13}\Psi)(\Psi^\dagger\gamma_{24}\Psi)\Big] - J\frac{(\Psi^\dagger\gamma_{14}\Psi)(\Psi^\dagger\gamma_{15}\Psi) - (\Psi^\dagger\gamma_{15}\Psi)(\Psi^\dagger\gamma_{23}\Psi) - (\Psi^\dagger\gamma_{13}\Psi)(\Psi^\dagger\gamma_{25}\Psi) - (\Psi^\dagger\gamma_{24}\Psi)(\Psi^\dagger\gamma_{25}\Psi)}{6\sqrt{3}} \\
\tilde{H}_{J2} &= \frac{J}{72}\Big[(\Psi^\dagger\Psi)^2 + 6(\Psi^\dagger\gamma_1\Psi)^2 + 6(\Psi^\dagger\gamma_2\Psi)^2 + 3(\Psi^\dagger\gamma_3\Psi)^2 + 4(\Psi^\dagger\gamma_5\Psi)^2 - (\Psi^\dagger\gamma_{12}\Psi)^2 - 2(\Psi^\dagger\gamma_{13}\Psi)^2 - 2(\Psi^\dagger\gamma_{14}\Psi)^2 \\
&\quad - 6(\Psi^\dagger\gamma_{15}\Psi)^2 - 2(\Psi^\dagger\gamma_{23}\Psi)^2 - 2(\Psi^\dagger\gamma_{24}\Psi)^2 - 6(\Psi^\dagger\gamma_{25}\Psi)^2 - 4(\Psi^\dagger\gamma_{34}\Psi)^2 - 3(\Psi^\dagger\gamma_{45}\Psi)^2\Big] \\
&\quad + \frac{J}{18}\Big[(\Psi^\dagger\gamma_{14}\Psi)(\Psi^\dagger\gamma_{23}\Psi) + (\Psi^\dagger\Psi)(\Psi^\dagger\gamma_5\Psi) - (\Psi^\dagger\gamma_{13}\Psi)(\Psi^\dagger\gamma_{24}\Psi) - (\Psi^\dagger\gamma_{12}\Psi)(\Psi^\dagger\gamma_{34}\Psi)\Big]
\end{aligned} \tag{S13}$$

1. *Fierz transformation*

Using Fierz identity we can decompose the particle-hole channel interactions into the pairing channel interactions. We will show that the repulsive particle hole channel interactions can be written in the form of attractive pairing channel terms through Fierz transformation.[13, 14] The required Fierz identity is,

$$(\Psi^\dagger M\Psi)(\Psi^\dagger N\Psi) = \frac{1}{16}\mathbf{Tr}[M^T\Gamma^A N\Gamma^B](\Psi^\dagger\Gamma^A\Psi^*)(\Psi^T\Gamma^B\Psi). \tag{S14}$$

	C_4	C_3	σ_h	σ_v	σ_d
γ_1	γ_2	γ_2	$-\gamma_1$	$-\gamma_1$	γ_2
γ_2	$-\gamma_1$	γ_3	$-\gamma_2$	γ_2	γ_1
γ_3	$-\gamma_3$	γ_1	γ_3	$-\gamma_3$	γ_3
γ_4	$-\gamma_4$	$-\frac{\gamma_4+\sqrt{3}\gamma_5}{2}$	γ_4	γ_4	$-\gamma_4$
γ_5	γ_5	$\frac{\sqrt{3}\gamma_4-\gamma_5}{2}$	γ_5	γ_5	γ_5

TABLE III. The table shows the transformation of $\gamma_i,\ i \in [1,5]$ under C_4 and C_3 rotations and reflections about the horizontal plane (σ_h), one of the vertical plane (σ_v) and dihedral plane (σ_d).

	I	γ_1	γ_2	γ_3	γ_4	γ_5	γ_{12}	γ_{13}	γ_{14}	γ_{15}	γ_{23}	γ_{24}	γ_{25}	γ_{34}	γ_{35}	γ_{45}
γ_{13}	1	1	1	1	1	1	−1	−1	−1	−1	−1	−1	−1	−1	−1	−1
$i\gamma_{13}\gamma_1$	1	1	−1	−1	−1	−1	1	1	1	1	−1	−1	−1	−1	−1	−1
$\gamma_{13}\gamma_2$	1	−1	1	−1	−1	−1	1	−1	−1	−1	1	1	1	−1	−1	−1
$i\gamma_{13}\gamma_3$	1	−1	−1	1	−1	−1	−1	1	−1	−1	1	−1	−1	1	1	−1
$\gamma_{13}\gamma_4$	1	−1	−1	−1	1	−1	−1	−1	1	−1	−1	1	−1	1	−1	1
$\gamma_{13}\gamma_5$	1	−1	−1	−1	−1	1	−1	−1	−1	1	−1	−1	1	−1	−1	1

TABLE IV. The table gives the values of $4C^{AA}_{N^TN}$ with rows representing the matrix N and column representing the matrix Γ^A.

Eq. (S14) are non-zero only for antisymmetric Γ matrices, i.e. $\Gamma \in \gamma_{13}, i\gamma_{13}\gamma_1, \gamma_{13}\gamma_2, i\gamma_{13}\gamma_3, \gamma_{13}\gamma_4, \gamma_{13}\gamma_5$.

Using these pieces of information, we construct a Table IV giving the values of $4C^{AA}_{N^TN}$ with rows representing the matrix N and column representing the matrix Γ^A where $\mathbf{Tr}[M^T\Gamma^A N\Gamma^B] = C^{AB}_{M^TN}$. After the Fierz transformation, the interactions with $M \neq N$ vanishes. From Table IV, we can write the projected interaction Hamiltonian terms in (S13) in pairing channel form as,

$$\begin{aligned}
\tilde{H}_U &= \frac{U}{24}[2(\Psi^\dagger(\gamma_{13})^\dagger\Psi^*)(\Psi^T\gamma_{13}\Psi) + (\Psi^\dagger(\gamma_{13}\gamma_4)^\dagger\Psi^*)(\Psi^T\gamma_{13}\gamma_4\Psi) + (\Psi^\dagger(\gamma_{13}\gamma_5)^\dagger\Psi^*)(\Psi^T\gamma_{13}\gamma_5\Psi)] \\
\tilde{H}_{U'} &= \frac{U'}{24}[(\Psi^\dagger(\gamma_{13})^\dagger\Psi^*)(\Psi^T\gamma_{13}\Psi) + 3(\Psi^\dagger(\gamma_{13}\gamma_1)^\dagger\Psi^*)(\Psi^T\gamma_{13}\gamma_1\Psi) + 3(\Psi^\dagger(\gamma_{13}\gamma_2)^\dagger\Psi^*)(\Psi^T\gamma_{13}\gamma_2\Psi) \\
&\quad + 3(\Psi^\dagger(\gamma_{13}\gamma_3)^\dagger\Psi^*)(\Psi^T\gamma_{13}\gamma_3\Psi) + 2(\Psi^\dagger(\gamma_{13}\gamma_4)^\dagger\Psi^*)(\Psi^T\gamma_{13}\gamma_4\Psi) + 2(\Psi^\dagger(\gamma_{13}\gamma_5)^\dagger\Psi^*)(\Psi^T\gamma_{13}\gamma_5\Psi)] \\
\tilde{H}_{J1} &= \frac{-J}{72}[3(\Psi^\dagger(\gamma_{13})^\dagger\Psi^*)(\Psi^T\gamma_{13}\Psi) + 3(\Psi^\dagger(\gamma_{13}\gamma_1)^\dagger\Psi^*)(\Psi^T\gamma_{13}\gamma_1\Psi) + 3(\Psi^\dagger(\gamma_{13}\gamma_2)^\dagger\Psi^*)(\Psi^T\gamma_{13}\gamma_2\Psi) \\
&\quad + 3(\Psi^\dagger(\gamma_{13}\gamma_3)^\dagger\Psi^*)(\Psi^T\gamma_{13}\gamma_3\Psi) + 6(\Psi^\dagger(\gamma_{13}\gamma_4)^\dagger\Psi^*)(\Psi^T\gamma_{13}\gamma_4\Psi) + 6(\Psi^\dagger(\gamma_{13}\gamma_5)^\dagger\Psi^*)(\Psi^T\gamma_{13}\gamma_5\Psi)] \\
\tilde{H}_{J2} &= \frac{J}{72}[12(\Psi^\dagger(\gamma_{13})^\dagger\Psi^*)(\Psi^T\gamma_{13}\Psi) - 3(\Psi^\dagger(\gamma_{13}\gamma_4)^\dagger\Psi^*)(\Psi^T\gamma_{13}\gamma_4\Psi) - 3(\Psi^\dagger(\gamma_{13}\gamma_5)^\dagger\Psi^*)(\Psi^T\gamma_{13}\gamma_5\Psi)]
\end{aligned} \tag{S15}$$

The total projected pairing interaction can be written as

$$\begin{aligned}
\tilde{H}_I &= \frac{2U+U'+3J}{24}(\Psi^\dagger\gamma_{13}^\dagger\Psi^*)(\Psi^T\gamma_{13}\Psi) + \frac{3U'-J}{24}[(\Psi^\dagger(\gamma_{13}\gamma_1)^\dagger\Psi^*)(\Psi^T\gamma_{13}\gamma_1\Psi) + (\Psi^\dagger(\gamma_{13}\gamma_2)^\dagger\Psi^*)(\Psi^T\gamma_{13}\gamma_2\Psi) \\
&\quad + (\Psi^\dagger(\gamma_{13}\gamma_3)^\dagger\Psi^*)(\Psi^T\gamma_{13}\gamma_3\Psi)] + \frac{U+2U'-3J}{24}[(\Psi^\dagger(\gamma_{13}\gamma_4)^\dagger\Psi^*)(\Psi^T\gamma_{13}\gamma_4\Psi) + (\Psi^\dagger(\gamma_{13}\gamma_5)^\dagger\Psi^*)(\Psi^T\gamma_{13}\gamma_5\Psi)]
\end{aligned} \tag{S16}$$

The first term in Eq. (S16) give rise to the singlet pairing while the remaining terms here correspond to the quintet pairing channel. We notice that the quintet pairing channel can be attractive in the strong Hund's coupling limit, whereas the single pairing channel is always repulsive.

B. Effect of Interband coupling between $j_{\text{eff}} = 3/2$ and $j_{\text{eff}} = 1/2$ bands

We now derive the effective many-body Hamiltonian induced by the interband coupling between $j_{\text{eff}} = 3/2$ and $j_{\text{eff}} = 1/2$ bands. To systematically calculate the effective Hamiltonian of $j_{\text{eff}} = 3/2$ band, we employ the many-body Schrieffer-Wolff transformation[15] and exact diagonalization technique.

1. Schrieffer-Wolff transformation

The Schrieffer-Wolff transformation decomposes the many-body interaction, H_I, into diagonal and off-diagonal component, $D(H_I)$ and $O(H_I)$ respectively, where each of them acts with the projection operator, P, to a target subsystem and its complementary space, $Q = 1 - P$. The diagonal and off-diagonal part can be written as,

$$\begin{aligned} D(H_I) &= PH_IP + QH_IQ \\ O(H_I) &= PH_IQ + QH_IP \end{aligned} \tag{S17}$$

In our case, we aim to derive the effective many-body interacting Hamiltonian of $j_{\text{eff}} = 3/2$ bands. Therefore, P projects to the target subspace, characterized by the quarter-filled electrons in $j_{\text{eff}} = 3/2$ bands and zero electrons in $j_{\text{eff}} = 1/2$ bands. The complementary space corresponds to the states with N electrons filled in $j_{\text{eff}} = 1/2$ bands and N electrons removed from quarter filled $j_{\text{eff}} = 3/2$ bands.

The effective Hamiltonian can be perturbatively expanded as[15],

$$\begin{aligned} H_{eff,1} &= PH_IP \\ H_{eff,2} &= \tfrac{1}{2}P[S_1, O(H_I)]p \\ H_{eff,3} &= \tfrac{1}{2}P[O(H_I), \mathcal{L}[D(H_I), S_1]]P \end{aligned} \tag{S18}$$

where we define a superoperator as $\mathcal{L}(X) = \sum_{i,j} \frac{\langle i|O(X)|j\rangle}{E_i - E_j} |i\rangle\langle j|$. The first-order term is just equal to the intra-band contributions considered in the previous section. The second-order describes the virtual many-body hopping processes as shown in Fig.S3(a). Other higher-order terms describe the more complicated virtual processes.

More specifically, we rewrite the interacting Hamiltonian in j_{eff} basis, which is written as,

$$H_I = \sum_{i_{1..4},k_1,k_2,q} V_{i_1 i_2 i_3 i_4} c^\dagger_{i_1}(k_1+q) c^\dagger_{i_2}(k_2-q) c_{i_3}(k_2) c_{i_4}(k_1) \tag{S19}$$

where $\vec{i} = (|\frac{1}{2}\,\frac{1}{2}\rangle, |\frac{1}{2}\,-\frac{1}{2}\rangle, |\frac{3}{2}\,\frac{3}{2}\rangle, |\frac{3}{2}\,\frac{1}{2}\rangle, |\frac{3}{2}\,-\frac{1}{2}\rangle, |\frac{3}{2}\,-\frac{3}{2}\rangle)$ indicates the j_{eff} basis. The second order effective Hamiltonian can be written as,

$$H_{eff,2} = \sum_{i_{1..4},k_1,k_2,q} V_{eff|i_1 i_2 i_3 i_4}(k_1,k_2,q) c^\dagger_{i_1}(k_1+q) c^\dagger_{i_2}(k_2-q) c_{i_3}(k_2) c_{i_4}(k_1) \tag{S20}$$

where the coupling constants can be computed from the eigenstates and the energy eigenvalues of the non-interacting Hamiltonian as,

$$\begin{aligned} V_{eff,2|i_1,i_2,i_3,i_4}(k_1,k_2,Q) = 2\sum_{j_{1,2,3,4},q_2} \Big(\frac{\theta(\epsilon_{j_3}(k_2-q_2))\theta(\epsilon_{j_4}(k_1+q_2))}{-\epsilon_{j_3}(k_2-q_2)-\epsilon_{j_4}(k_1+q_2)}\Big) W_{i_1,i_2,j_3,j_4}(k_1+q_2, k_2-q_2, Q-q_2) \\ \times W_{j_1,j_2,i_3,i_4}(k_1,k_2,q_2)(\delta_{j_3,j_2}\delta_{j_4,j_1}) OR(j_3 \le 2, j_4 \le 2) \end{aligned} \tag{S21}$$

where $W(k_1,k_2,q)(k_1,k_2,q)$ is the interaction coefficient in the energy eigenstate basis. θ is the heavi-side step function. ϵ_i is the energy eigenvalue of i-th non-interacting band. By numerically plugging in the information of the non-interacting bands, we find that the second-order interband tunneling always contributes as the attractive singlet and quintet pairing interactions. This result becomes analytically apparent if we consider the flat band limit. In this limit, $H_{\text{eff},2}$ can be explicitly calculated as,

$$g_{\text{eff},0} = -\frac{1}{18}\frac{(3J_H + U - U')^2}{\Delta E} \quad g_{\text{eff},1} = -\frac{1}{6}\frac{J_H^2}{\Delta E}, \quad g_{\text{eff},2} = -\frac{1}{24}\frac{(U-U')^2}{\Delta E}, \tag{S22}$$

where ΔE is the band splitting between $j_{\text{eff}} = 3/2$ and $1/2$ bands. As a result, we find that the leading order corrections are all negative, which contributes as an attractive pairing channel. This result is irrespective of the specific values of (U, U', J_H), since they are the complete square form.

The exact interband tunneling contribution can be numerically computed up to all orders using the exact-diagonalization technique in the flat band limit. Fig. S3(b) shows the effective pairing strength derived from the exact diagonalization technique as a function of the interband splitting between $j_{\text{eff}} = 3/2$ and $j_{\text{eff}} = 1/2$. We find that the decrease of the interband spacing increases the effect of the interband tunneling, finally contributing as negative correction of g_1 Especially, when the fully screened interaction is taken into account, we find that the pairing interaction strength can turn to a negative value. Eventually, the attractive superconducting pairing channels open. In results, we conclude that the reduction of the band splitting in addition to the strong Hund's coupling may induce the quintet pairing superconductivity in $j_{\text{eff}} = 3/2$ bands.

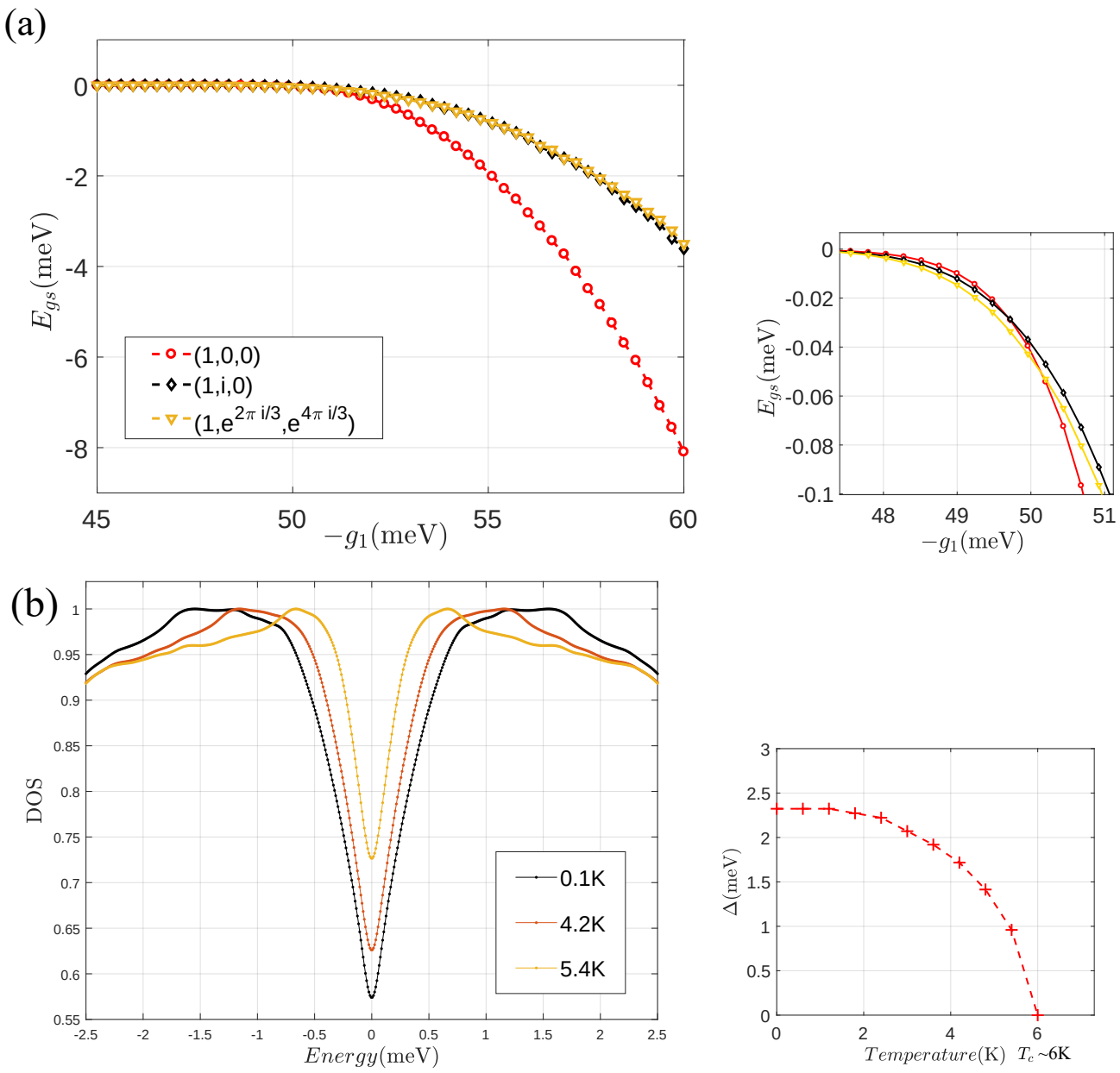

FIG. S4. (a) Total energy calculation derived from the mean-field theory as a function of g_1. The superconducting order parameters are represented as three component vectors. Inset: magnified figure around $-g_1 \approx 50$meV. we find the phase transition from the time-reversal broken phase to the time-reversal symmetric phase. (b) The density of states of $(1,0,0)$-pairing as a function of the temperature. Nodal line superconductivity shows the linear DOS profile. Inset: (1,0,0) order parameter dependence as a function of the temperature. Using the critical temperature $T_c \sim 6$K, we expect the formation of 2.4meV superconducting order parameter at zero temperature.

4. MEAN-FIELD ENERGY CALCULATION

In the previous section, we find that the pairing channel with t_{2g} symmetry can be attractive when the high pressure is applied. Based on this observation, we perform the standard mean-field theory calculation of the superconductivity. We compare the possible order parameter configurations with t_{2g} symmetry: time-reversal symmetric $(1,0,0)$-state, time-reversal broken $(1,i,0)$-state, and $(1,e^{2\pi i/3},e^{4\pi i/3})$-state. Fig. S4(a) compares the corresponding ground state energies. In the weak coupling limit where $-g_1 < 50$meV, we find that the time-reversal broken $(1,e^{2\pi i/3},e^{4\pi i/3})$state is the most energetically favored ground state(See inset for the magnified figure). As g_1 is further increased, the

phase transition from the time-reversal broken phase to the time-reversal symmetric phase is observed. In particular, $GaTa_4Se_8$ has the critical temperature of $T_c \sim 5.8$K, where the corresponding energy scale, $E_{gs} \sim 0.5$meV, is well outside the phase transition point in Fig. 1 (b). Therefore, we conclude that the time-reversal symmetric $(1,0,0)$-pairing is the relevant ground state and perform further analysis assuming $(1,0,0)$-state in the main text.

Nevertheless, we also note that the time-reversal broken states can be realizable near the phase transition where the order parameter is suppressed. In such a case, the gap structure of the time-reversal broken states are generally characterized by the Bogoliubov Fermi surfaces. This time-reversal broken states have been similarly found in the previous studies of Luttinger semimetal[13, 16–21]. However, we also note the important difference with the Luttinger semimetal that $GaTa_4Se_8$is a quarter filled material where the Fermi level lies at the center of the $j_{\text{eff}} = 3/2$ valence band.

As explained in the main text, $(1,0,0)$ pairing state is characterized by d_{xy}-wave nodal line gap structure. Fig. S4 (b) shows the density of states(DOS) profile of $(1,0,0)$ pairing state with $T_c = 5.8$K as a function fo the temperature. Due to the presence of the nodal lines, the DOS profile shows a linear nodal behavior rather than the full gap. This difference with the BCS superconductivity can be directly observed from the tunneling spectroscopy.

5. DETAILS OF TRANSPORT CALCULATION

To model the Josephson junction, we introduce the four band model of the s-wave BCS superconductor. The BdG Hamiltonian describing the BCS superconductor is given as,

$$H_{BCS}(\mathbf{k}) = \begin{pmatrix} [-2t_0(cos(k_x)+cos(k_y)+cos(k_z))-\mu]I_4 & |\Delta|e^{i\phi}\gamma_{13} \\ |\Delta|e^{-i\phi}\gamma_{13} & -[-2t_0(cos(k_x)+cos(k_y)+cos(k_z))-\mu]I_4 \end{pmatrix}, \quad \text{(S23)}$$

where μ is the chemical potential. ϕ is the order parameter phase difference between the lacunar spinel and the BCS superconductor. To model the tunneling junction, we introduce the tunneling term between the Lacunar spinel and the BCS superconductor as,

$$H_{tunneling} = \sum_{i \in junction} t_0 \Psi_i^\dagger I_4 c_i, \quad \text{(S24)}$$

where Ψ and c indicate the four component spinors of the lacunar spinel and the BCS superconductor. the site index i is summed over the junction region. After constructing the tight-binding model of the Josephson junction, we numerically diagonalize the occupied energy of the tight binding model while varying the phase difference, ϕ. This procedure gives the free energy, $F(\phi)$, as a function of ϕ, and the Josephson current is given as $I_J(\phi) = \frac{2e}{\hbar}\frac{dF(\phi)}{d\phi}$. Finally, we derive the current-phase relation of the planar Josephson junction by gradually rotating the orientation of the junction.

[1] Pocha, R., Johrendt, D., Ni, B. & Abd-Elmeguid, M. M. Crystal structures, electronic properties, and pressure-induced superconductivity of the tetrahedral cluster compounds $GaNb_4S_8$, $GaNb_4Se_8$, and $GaTa_4Se_8$. *Journal of the American Chemical Society* **127**, 8732–8740 (2005). PMID: 15954779.

[2] Kotani, T. first-principles electronic structure calculation code, ecalj package (https://github.com/tkotani/ecalj).

[3] Kim, H.-S., Im, J., Han, M. J. & Jin, H. Spin-orbital entangled molecular j_{eff} states in lacunar spinel compounds. *Nature communications* **5**, 3988 (2014).

[4] Aryasetiawan, F. *et al.* Frequency-dependent local interactions and low-energy effective models from electronic structure calculations. *Physical Review B* **70**, 195104 (2004).

[5] Şaşıoğlu, E., Friedrich, C. & Blügel, S. Effective Coulomb interaction in transition metals from constrained random-phase approximation. *Phys. Rev. B* **83**, 121101 (2011).

[6] Miyake, T. & Aryasetiawan, F. Screened Coulomb interaction in the maximally localized Wannier basis. *Phys. Rev. B* **77**, 085122 (2008).

[7] Aryasetiawan, F., Karlsson, K., Jepsen, O. & Schnberger, U. Calculations of Hubbard U from first-principles. *Physical Review B* **74**, 125106 (2006).

[8] Vaugier, L., Jiang, H. & Biermann, S. Hubbard U and Hund exchange J in transition metal oxides: Screening versus localization trends from constrained random phase approximation. *Physical Review B* **86**, 165105 (2012).

[9] Sakuma, R. & Aryasetiawan, F. First-principles calculations of dynamical screened interactions for the transition metal oxides MO (M= Mn, Fe, Co, Ni). *Physical Review B* **87**, 165118 (2013).

[10] Miyake, T., Aryasetiawan, F. & Imada, M. Ab initio

procedure for constructing effective models of correlated materials with entangled band structure. *Phys. Rev. B* **80**, 155134 (2009).

[11] Panda, S. K., Jiang, H. & Biermann, S. Pressure dependence of dynamically screened Coulomb interactions in NiO: effective Hubbard, Hund, intershell, and intersite components. *Phys. Rev. B* **96**, 045137 (2017).

[12] Kim, H.-S., Haule, K. & Vanderbilt, D. Molecular Mott state in the deficient spinel GaV_4S_8 (2018). 1810.09495.

[13] Boettcher, I. & Herbut, I. F. Unconventional superconductivity in Luttinger semimetals: theory of complex tensor order and the emergence of the uniaxial nematic state. *Phys. Rev. Lett.* **120**, 057002 (2018).

[14] Sim, G. *et al.* Topological d+ s wave superconductors in a multiorbital quadratic band touching system. *Physical Review B* **100**, 064509 (2019).

[15] Bravyi, S., DiVincenzo, D. P. & Loss, D. Schrieffer–Wolff transformation for quantum many-body systems. *Annals of physics* **326**, 2793–2826 (2011).

[16] Menke, H., Timm, C. & Brydon, P. M. R. Bogoliubov Fermi surfaces stabilized by spin-orbit coupling. *Phys. Rev. B* **100**, 224505 (2019).

[17] Savary, L., Ruhman, J., Venderbos, J. W. F., Fu, L. & Lee, P. A. Superconductivity in three-dimensional spin-orbit coupled semimetals. *Phys. Rev. B* **96**, 214514 (2017).

[18] Agterberg, D. F., Brydon, P. M. R. & Timm, C. Bogoliubov Fermi surfaces in superconductors with broken time-reversal symmetry. *Phys. Rev. Lett.* **118**, 127001 (2017).

[19] Roy, B., Ghorashi, S. A. A., Foster, M. S. & Nevidomskyy, A. H. Topological superconductivity of spin-3/2 carriers in a three-dimensional doped Luttinger semimetal. *Phys. Rev. B* **99**, 054505 (2019).

[20] Venderbos, J. W. F., Savary, L., Ruhman, J., Lee, P. A. & Fu, L. Pairing states of spin-$\frac{3}{2}$ fermions: symmetry-enforced topological gap functions. *Phys. Rev. X* **8**, 011029 (2018).

[21] Brydon, P. M. R., Wang, L., Weinert, M. & Agterberg, D. F. Pairing of $j = 3/2$ Fermions in Half-Heusler Superconductors. *Phys. Rev. Lett.* **116**, 177001 (2016).